CHARACTERIZATION OF NATIVE VACANCIES IN EPITAXIAL GaN AND ZnSe SEMICONDUCTOR LAYERS BY POSITRON ANNIHILATION SPECTROSCOPY

Juha Oila

Laboratory of Physics
Helsinki University of Technology

Fysiikan laboratorio
Teknillinen korkeakoulu

DISSERTATION 117 (2002)

CHARACTERIZATION OF NATIVE VACANCIES IN EPITAXIAL GaN AND ZnSe SEMICONDUCTOR LAYERS BY POSITRON ANNIHILATION SPECTROSCOPY

Juha Oila

Laboratory of Physics
Helsinki University of Technology
Espoo, Finland

Dissertation for the degree of Doctor of Science in Technology to be presented with due permission of the Department of Engineering Physics and Mathematics for public examination and debate in Council Room at Helsinki University of Technology (Espoo, Finland) on the 15th of November, 2002, at 13 o'clock.

Dissertations of Laboratory of Physics, Helsinki University of Technology
ISSN 1455-1802

Dissertation 117 (2002):
Juha Oila: Characterization of Native Vacancies in Epitaxial GaN
and ZnSe Semiconductor Layers by Positron Annihilation Spectroscopy
ISBN 951-22-6182-0 (print)
ISBN 951-22-6183-9 (electronic)

OTAMEDIA OY
ESPOO 2002

Abstract

Point defects in epitaxial GaN and ZnSe semiconductor layers have been studied using a low-energy positron beam. Ga vacancies are found to be present in n-type GaN grown by metal organic chemical vapor deposition, where the conductivity is due to residual oxygen. When n-type silicon impurity doping is done, clearly less vacancies are observed. In Mg-doped p-type and semi-insulating materials the vacancies are not observed. In GaN layers grown by molecular-beam epitaxy also bigger vacancy clusters are detected. The formation of Ga vacancies is found to depend strongly on the stoichiometry during the growth, and much less on the structural quality of the layers. In GaN layers positrons are trapped also at edge-type dislocations, which are shown to be negatively charged but not to contain open-volume defects.

Undoped Znse layers are found to contain negative Zn vacancies. In nitrogen doped ZnSe and $ZnS_{0.06}Se_{0.94}$ layers Se vacancies are detected. These are most likely part of a defect complex with N impurity. Positron trapping at negative N acceptors is also observed. By combining the results of positron annihilation, secondary ion mass spectrometry, and capacitance-voltage measurements, a detailed picture of the deactivation of N impurities in ZnSe is obtained.

Preface

This thesis has been prepared in the Laboratory of Physics at Helsinki University of Technology during the years 1998-2002. I wish to thank my supervisor Professor Pekka Hautojärvi for the opportunity to work in the positron physics group. I appreciate greatly the solid background he has provided in physics and especially in the field of positron spectroscopy whenever it has been needed.

I express my sincere gratitude to Professor Kimmo Saarinen for advising my thesis. He has given me the essential insight into my work, and his optimistic and open-minded outlook on research problems has invaluably promoted this work.

Working in the experimental positron group with talented, inspiring, and helpful people has been a great privilege. Most of all, I want to thank Dr. Jaani Nissilä and Dr. Tatu Laine for the detailed introduction into experimental methods, and Dr. Klaus Rytsölä for his assistance in technical problems. I have gained very much from the collaboration with Ville Ranki, Jani Kivioja, Sami Hautakangas, and our French colleagues, Dr. Pierre Desgardin and Dr. Laurent Henry. The discussions with Dr. Jonatan Slotte, Antti Laakso, Lauri Salminen, Reino Aavikko, Antti Pelli, and with all the other people downstairs have been very fruitful.

It is my pleasure to thank the whole staff of the laboratory for creating an enjoyable working atmosphere. Especially Mrs. Eija Järvinen, Mr. Kaarle Tahvanainen, Mr. Heikki Vaalte, and Mr. Eero Turtiainen are acknowledged for all their help during these years.

Finally, I want to thank my parents, brothers, sisters, and friends for all the support and joy they have given to me.

Otaniemi, September 2002

Juha Oila

Contents

List of publications

This thesis consists of an overview and the following publications:

I. K. Saarinen, P. Seppälä, J. Oila, P. Hautojärvi, C. Corbel, O. Briot, and R. L. Aulombard, *Gallium vacancies and the growth stoichiometry of GaN studied by positron annihilation spectroscopy*, Applied Physics Letters **73**, 3253 (1998).

II. J. Oila, V. Ranki, J. Kivioja, K. Saarinen, P. Hautojärvi, J. Likonen, J. M. Baranowski, K. Pakula, T. Suski, M. Leszczynski, and I. Grzegory, *Influence of dopants and substrate material on the formation of Ga vacancies in epitaxial GaN layers*, Physical Review B **63**, 045205 (2001).

III. P. Laukkanen, S. Lehkonen, P. Uusimaa, M. Pessa, J. Oila, S. Hautakangas, K. Saarinen, J. Likonen, and J. Keränen, *Structural, electrical, and optical properties of defects in Si-doped GaN grown by molecular-beam epitaxy on hydride vapor phase epitaxy GaN on sapphire*, Journal of Applied Physics **92**, 786 (2002).

IV. J. Oila, K. Saarinen, A. E. Wickenden, D. D. Koleske, R. L. Henry, and M. E. Twigg, *Ga vacancies and grain boundaries in GaN*, submitted for publication in Applied Physics Letters.

V. P. Desgardin, J. Oila, K. Saarinen, P. Hautojärvi, E. Tournié, J.-P. Faurie, and C. Corbel, *Native vacancies in nitrogen-doped and undoped ZnSe layers studied by positron annihilation*, Physical Review B **62**, 15711 (2000).

VI. J. Oila, K. Saarinen, T. Laine, P. Hautojärvi, P. Uusimaa, M. Pessa, and J. Likonen, *Experimental identification of the doping deactivation mechanism in semiconductors: Application to nitrogen in* $ZnS_{0.06}Se_{0.94}$, Physical Review B: Rapid communication **59**, 12736 (1999).

VII. J. Oila, V. Ranki, J. Kivioja, K. Saarinen, and P. Hautojärvi, *Target chamber for a slow positron beam: optimization of count rate and minimization of backscattering effects*, Applied Surface Science **194**, 38 (2002).

The roman numerals are used in this overview when referring to the publications.

The author's contribution

The author has had an active role in all stages of the work reported in this thesis. He has been involved in the planning and performing of the experiments as well as in the analysis of the experimental data, and he has contributed to the interpretation of the results. The author has written Publications II, IV, VI, VII, and the section considering positron annihilation experiments in Publ. III, and he has the main responsibility for the work reported in them.

1 Introduction

The electrical conductivity of semiconductors is controlled by incorporating appropriate impurity atoms into the lattice. These dopant atoms create donor or acceptor states in the band-gap, generating the population of free charge carriers, electrons or holes. During the material fabrication various point and extended defects can be formed in the semiconductor lattice. The localized electronic states related to these defects may limit the characteristics of the material, e.g. by acting as scattering or recombination centers for the charge carriers or by compensating the dopant atoms. The formation of defects is influenced by the stoichiometry of the growth conditions and by the position of the Fermi level in the energy gap. The electronic and optical quality of a semiconductor is largely determined by the properties and the amount of the native defects and impurities. The detailed knowledge on the formation and the nature of the defects is therefore needed for high performance applications.

Optoelectronic semiconductor devices, e.g. light-emitting diodes and laser diodes, have an important role in many applications of telecommunication and information technology. During the recent years, much effort has been put to develope semiconductor devices working in the short wavelength, blue light, region. Gallium nitride and zinc selenide both have a direct wide band-gap and are potential materials for short wavelength applications.

The rapid progress in GaN-based semiconductor technology has already led to the commercial launching of optoelectronic components. Many of the material properties and characteristics are, however, not fully understood. The growth of large size bulk GaN crystals is very difficult. The device-quality GaN is typically grown epitaxially on sapphire (Al_2O_3) substrate. The lattice-mismatch between the GaN layer and the sapphire substrate may, however, lead to dislocation densities as high as 10^{10} cm^{-2} threading through the GaN layer. Several experimental and theoretical studies suggest that the dislocation lines are electrically and optically active [1, 2, 3].

The most important native point defects in GaN are calculated to be the vacancies [4]. In n-type GaN the most probable defect is the gallium vacancy. The gallium vacancy V_{Ga} acts as a deep acceptor [5] and is suggested to be responsible for the carrier compensation in n-type GaN [6]. In addition to the formation of isolated Ga vacancies, also the formation of complexes between the Ga vacancy and oxygen or silicon donor-impurities is calculated to be energetically favored [5, 7]. In GaN devices a parasitic broadband component is commonly observed in the yellow part of the emission spectrum. The acceptor states created by the Ga vacancy or Ga vacancy related complexes are suggested also to be involved in this yellow luminescence [5, 7]. The nitrogen vacancy is reported to act as a shallow donor in GaN [8], and it is suggested to behave as a potential compensating defect in Mg-doped GaN grown at high temperatures [9].

The realization of high-quality ZnSe-based devices has been restricted by fundamental problems in material fabrication. One of the major difficulties is the strong compensation of p-type doping. The best results are obtained with nitrogen as an acceptor impurity. The charge carrier concentrations have been found, however, to saturate at about $\leq 10^{18}$ cm^{-3} regardless of much larger amount of incorporated nitrogen atoms. It has been proposed that the deactivation of acceptors could be caused by the formation of dopant impurity–native

defect pairs [10], creation of N_2 molecules [11], or dopant atom related lattice instability which turns a shallow acceptor level into a deep one [12]. Heteroepitaxial growth, typically on GaAs substrates, gives as well rise to problems due the lattice mismatch between GaAs and ZnSe. ZnSe-based devices are found to degrade during the operation, leading to shortened device lifetimes. The degradation process has been suggested to be related to the formation of both extended and point defects [13, 14].

In this work we have studied vacancy-type defects in epitaxial GaN and ZnSe layers using a low-energy positron beam. Positron annihilation is an effective tool for studying vacancy-type defects in semiconductors [15, 16, 17]. Positrons get trapped at vacancies due to the missing positive ion core at vacancy site [18]. The trapping is experimentally observed in two ways: as a narrowing of the momentum distribution of the annihilating electron-positron pair and as an increase in the positron lifetime. The annihilation data gives information on the nature of the atoms around the vacancy and enables distinguishing between vacancies in different sublattices.

In Publications I and II we have studied the influence of doping and stoichiometry on the formation of Ga vacancies in GaN. Ga vacancies are detected at high concentrations in GaN which is n-type due to residual oxygen impurities. The concentration of V_{Ga} increases strongly when the V/III molar ratio is increased in the metal-organic chemical vapor deposition (MOCVD) growth. In p-type and in semi-insulating layers Ga vacancies are not found. In GaN layers grown by molecular-beam epitaxy (MBE) we observe also bigger vacancy clusters [III]. The dependence between Ga vacancies and dislocations is studied in Publ. IV. We find no obvious correlation between the vacancy concentration and the dislocation density. The data suggest that the dislocations are negatively charged, but do not contain vacancies.

The investigation of ZnSe and $ZnS_{0.06}Se_{0.94}$ layers are reported in Publications V and VI. In undoped ZnSe layers we identify Zn vacancies. In N-doped material positrons are trapped at Se vacancies, which are most likely in complex with N impurity. Positrons are trapped also at negative ions, which are attributed to isolated N acceptors. By combining the positron data with the results of capacitance-voltage (CV) and secondary ion mass spectrometry (SIMS) measurements, the deactivation of N acceptors is shown to be due to the formation of compensating nitrogen related defect complexes and, in some layers, due to incorporation of nitrogen in electrically neutral form.

A modification of the positron beam facility is reported in Publ. VII. The magnetic field at the sample position was increased by using permanent magnets. The increased field focuses the beam and guides effectively away the backscattered positrons, which otherwise would cause error in the positron annihilation parameters.

2 Experimental methods

Positron annihilation spectroscopy is a method to detect and identify open-volume defects, such as vacancies and voids, in solid material [15, 16, 17]. Positrons are implanted into the sample material where they annihilate with electrons. As a positive particle, positron tends to get trapped at vacancy sites. The experimental information is obtained by detecting the 511 keV annihilation photons which are emitted in the annihilation process. The lifetime of the positron gives information on the electron density in the sample material, as encountered by the positron. In the annihilation process momentum is conserved. The momentum of the annihilating positron–electron pair can be observed as a Doppler shift in the energy of the annihilation photons and as a small angular deviation from the 180° angle between the two photons. In this thesis, the characterization of defects is based on the Doppler-broadening measurements.

After implantation into a solid material, positrons loose their energy until they are in thermal equilibrium with the surrounding matter. The thermalization process is very fast, taking only a few picoseconds, as compared to the average positron lifetime which is typically around 200 ps in semiconductors. Thermalized positrons diffuse in the lattice until they annihilate with an electron. In absence of defects which could trap the positron, the diffusion is limited mainly by phonon scattering, as scattering from electrons and lattice defects have a minor role. Typical positron diffusion length in semiconductors is of the order of 100 nm at room temperature.

In a perfect semiconductor lattice positrons can be described by a delocalized Bloch-like wavefunction, which has its maximum amplitude between the repulsive positive ion cores. Open-volume defects, e.g. vacancies and bigger voids, where positive ion cores are missing, may trap positrons into a localized state. Trapping is possible only at neutral or negatively charged vacancies; the Coulombic repulsion prevents trapping at positive vacancies. The positron binding energy at vacancy-type defects is of the order of 1 eV. The trapping rate at the vacancies, κ_V, is proportional to the concentration of the vacancies: $\kappa_V = c_V \, \mu_V / N_{at}$, where μ_V is the vacancy specific trapping coefficient and N_{at} is the atomic density of the material. Positrons are also sensitive to negative ion-type defects, e.g. ionized acceptors in semiconductors. Positrons get trapped at Rydberg levels around negative ions. The binding energy at these shallow traps is typically < 100 meV, and thus the trapping is effective only at low temperatures.

At a vacancy the average electron density is lower than in the bulk lattice, leading to an increase in the lifetime of trapped positrons. The vacancy specific lifetime τ_V depends on the size of the vacancy. The measurement of the positron lifetime spectrum can be used to identify different vacancies and to give information on their concentration. Also the average momentum of electrons at the vacancy site is reduced. The positron trapping at vacancies leads to a narrower momentum distribution of annihilating positron-electron pairs than free positron annihilation in the lattice. This can be observed by measuring the Doppler-broadening of the 511 keV annihilation line. The high-momentum part of the momentum distribution is caused almost totally by the annihilations with atomic core electrons. The core electron momentum distribution gives thus information about the chemical nature of atoms around the annihilation site and can be used to distinguish between vacancies in different sublattices.

The Doppler broadening of the 511 keV annihilation line is measured by a high-resolution Ge-detector. The broadening is characterized by line shape parameters, the low-momentum parameter S and the high-momentum parameter W. The S parameter measures the fraction of counts in the central part of the 511 keV peak, corresponding to a longitudinal momentum component of $p_L \leq 3.7 \times 10^{-3}\ m_0c$ (± 0.95 keV around the peak center), thus representing mainly the annihilations with valence electrons. The W parameter is the fraction of counts in the wing areas of the peak, $11 \times 10^{-3}\ m_0c \leq p_L \leq 29 \times 10^{-3}\ m_0c$, describing annihilations with high momentum core electrons. The narrower momentum distribution caused by positron trapping at vacancies is seen as an increase in the S parameter and as a decrease in the W parameter.

The annihilation parameters recorded in a particular sample are superpositions of parameters characterizing annihilations at different positron states, weighted with corresponding annihilation fractions η. If only one type of vacancy, which traps positrons, is present in the lattice, the measured S and W parameters are linear combinations of values (S_b, W_b) corresponding to the annihilation as a free positron in the defect-free bulk lattice and values (S_V, W_V) characterizing the annihilations of the positrons trapped at vacancies,

$$S = (1 - \eta_V)\, S_b + \eta_V\, S_V \quad \text{and} \tag{1}$$

$$W = (1 - \eta_V)\, W_b + \eta_V\, W_V\,. \tag{2}$$

In S–W plane the (S, W) points fall on the line between the points (S_b, W_b) and (S_V, W_V) and the exact position is determined by the fraction of trapped positrons. The inverse slope of the line, $R_V = |\Delta S/\Delta W| = |(S_V - S_b)/(W_V - W_b)|$, is a defect specific parameter and it can be used to distinguish between different vacancies [19].

By introducing κ_V, the positron trapping rate, and λ_b, the positron annihilation rate from the delocalized state, into Eq. (1),

$$S = \frac{\lambda_b}{\lambda_b + \kappa_V}\, S_b + \frac{\kappa_V}{\lambda_b + \kappa_V}\, S_V\,, \tag{3}$$

the concentration of vacancies can be determined as

$$c_V = \frac{N_{at}}{\mu_V\, \tau_b} \frac{(S - S_b)}{(S_V - S)}\,. \tag{4}$$

Here $\tau_b = 1/\lambda_b$ is the positron lifetime in a defect-free lattice. If positrons are trapped both at vacancies and at Rydberg states around negative ions, the S parameter is

$$S = \frac{1}{\lambda_b + \kappa_V + \frac{\kappa_{ion}}{1+\delta_{ion}}} (\lambda_b\, S_b + \kappa_V\, S_V + \frac{\kappa_{ion}}{1 + \delta_{ion}}\, S_{ion})\,, \tag{5}$$

where $\kappa_{ion} = c_{ion}\, \mu_{ion}/N_{at}$ is the trapping rate at the negative ions and δ is the thermal detrapping rate from the ions. As the surroundings of negative ions do not contain open volume, the characteristic S parameter $S_{ion} = S_b$.

The annihilation parameters S and W are characteristic to each material. Their absolute values, however, depend on the energy resolution of the detector system and on the chosen energy window used for counting the pulses. A well known reference sample, preferably a sample with no positron traps in it, is therefore needed for comparing the results

between different experimental set-ups and for determining the bulk values S_b and W_b. For the estimation of the vacancy concentration, the vacancy specific parameters S_V and W_V have to be known. They can be determined e.g. by comparing the results of the Doppler broadening measurements and the positron lifetime experiments, or by studying a sample with a very high concentration of vacancies ($\eta_V = 1$).

Positrons, which are emitted in the β^+-decay of radioactive nuclei, are highly energetic and have a continuous energy spectrum, which leads to a wide penetration depth distribution in the sample material. The average penetration depth of positrons from ^{22}Na source is tens of micrometers in a semiconductor lattice. The characterization of thin epitaxial layers is done using a low-energy positron beam. In a low-energy positron beam positrons are first slowed down and then accelerated by an electric field to form a monoenergetic beam with adjustable energy.

In the positron beam facility the positron source and the sample are located in vacuum chambers. Positrons hit a thin moderator foil (single crystal W), where they become thermalized. Due to the negative work function in tungsten, the thermalized positrons which reach the surface of the foil are emitted to the vacuum with the energy corresponding the work function, ~ 3 eV. The positrons, which have transmitted the foil, are extracted and focused by a small voltage to the beamline. In the beamline the positrons are guided by axial magnetic field. The moderation efficiency of the foil is low, $< 10^{-4}$, and before the acceleration to the final energy, a velocity selector is used to filter the non-thermalized positrons away from the beam. The final beam energy can be adjusted between 0 and 40 keV. This enables the depth scan of the semiconductor layer from the topmost atom layers down to a depth of few micrometers.

During the experiments of this work a new target chamber (Fig. 1) was designed [VII]. The new chamber allows Doppler broadening measurements with two Ge detectors in coincidence. In the design a special care was taken to minimize the effect of backscattered positrons. The two-detector coincidence set-up is used to remove the background radiation from the Doppler spectrum. The detectors are situated on opposite sides of the sample and only those events, when both 511 keV photons are detected, are accepted. The discrimination can be done either using a scintillator detector, NaI or BGO, with the Ge detector, or by using two Ge detectors to record the energy of both photons [20, 17]. This technique allows the analysis of the positron–electron momentum distribution up to a momentum of 60 m_0c.

A portion of the positrons which hit the target surface are scattered back to the vacuum. The backscattered positrons, which hit the wall of the vacuum chamber near the detector, may cause a systematic error in the annihilation spectrum. The effect of the backscattered positrons becomes stronger at higher positron incident energies: First, the total backscattering probability increases with incident energy, and second, when a positron scatters away from the target with a high velocity component in a direction perpendicular to the field direction, the magnetic field cannot effectively guide the positrons away from the vicinity of the detectors. This comes especially severe in the two detector set-up, as the sample is surrounded by both sides by the detector noses, which are brought very close to the sample in order to maximize the count rate.

In the new chamber we have mounted strong permanent magnets (NdFeB) behind the sample holder. These increase the magnetic flux density in the critical area between the

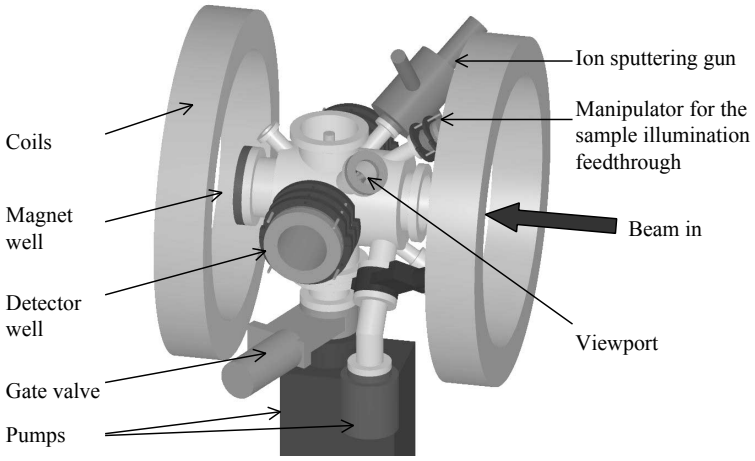

Figure 1: An overall view of the new target chamber [Publ. VII].

detectors. In addition, the distance between the target and the detector wells can be adjusted. This enables to compromize between the count rate and the number of backscattered positrons annihilating at the end plates of the well.

The test measurements showed, that the increased magnetic field effectively guides the backscattered positrons away from the vicinity of the detectors. The distortion caused by the backscattered positrons could not be seen at any positron energies. The increase in the flux density also focuses the beam leading to a smaller spot size.

3 Native vacancies in GaN epitaxial layers

3.1 Ga vacancies in GaN grown on sapphire by MOCVD

According to theoretical calculations [4], the most important point defects in GaN are vacancies: the dominating native defect in p-type GaN is expected to be the N vacancy and in n-type GaN the Ga vacancy. The formation energy of antisites and interstitials has been found to be too high for them to exist in significant concentrations.

3.1.1 Influence of dopants on the vacancy formation

The p-type doping of GaN is usually done with Mg-impurities. After the growth the GaN:Mg grown by metal-organic chemical vapor deposition (MOCVD) is highly compensated and the p-type conductivity is achieved after thermal treatment. The n-type doping is more straightforward, both oxygen or silicon impurities can be used as n-type dopants. Undoped GaN shows usually high n-type conductivity, which is most commonly associated to residual oxygen [4, 21]. To study the influence of doping on the formation of native vacancies, we investigated Mg-doped p-type and semi-insulating (SI) layers, nominally undoped layers, and Si-doped n-type layers, which were grown on Al_2O_3 substrate by MOCVD. As a reference sample, we studied a heavily Mg-doped GaN single crystal. In this bulk crystal positron lifetime experiments [22] yield a single lifetime component of 165 ps, which corresponds to positron annihilation in delocalized state in the GaN lattice.

The p-type conductivity, $p = 2 \times 10^{17}$ cm^{-3}, in the Mg-doped layer has been achieved

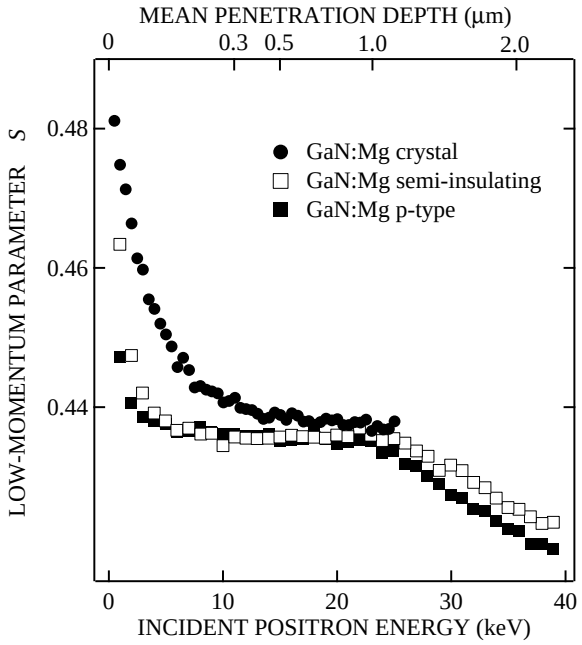

Figure 2: The low-momentum parameter S as a function of the incident positron energy in p-type and semi-insulating Mg-doped layers and in Mg-doped GaN bulk crystal. The positron mean penetration depth is indicated by the top axis [Publ. II].

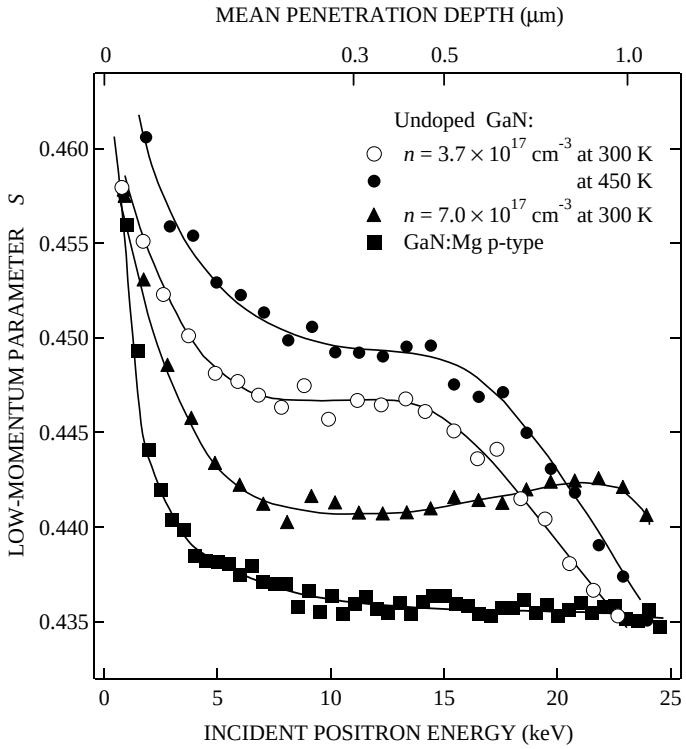

Figure 3: The low-momentum parameter S vs. positron incident energy in two undoped GaN layers. The solid lines are guides to the eye [Publ. II].

by post-growth thermal annealing. In the semi-insulating (SI) sample the heavy Mg-doping without thermal annealing compensates the residual n-type conductivity. In Fig. 2 are shown the S parameters in p-type and SI layers, together with the curve measured in p-type reference crystal. In both epitaxial layers the plateau of the constant $S \approx 0.435$, observed in the energy range 5-25 keV, characterizes the annihilations inside the GaN layer. At higher positron energies part of the positrons annihilate in Al_2O_3 substrate leading to a decrease in S. At low positron energies, $E < 5$ keV, more positrons are able to diffuse onto the sample surface, and the S parameter increases towards the value characteristic to annihilations at the surface.

The layer-specific parameters both in semi-insulating and in p-type GaN layers are equal to those measured in Mg-doped reference crystal, indicating that in Mg-doped layers the positrons are not trapped at vacancies. This conclusion is supported also by the temperature behaviour of the annihilation parameters, which show only small variation in the temperature range between 30 and 600 K [II], as typically observed for positron annihilation in defect-free lattice [16].

The studied nominally undoped GaN layers show strong n-type conductivity with $n = 10^{17}$–10^{18} cm^{-3}. According to the SIMS measurements the concentration of oxygen in epitaxial layers was $> 10^{18}$ cm^{-3}, which is enough to explain the n-type conductivity. Figure 3 shows the $S(E)$ curves in two undoped GaN layers. A plateau of the S parameter which characterizes the annihilations inside 0.6 and 1 μm thick layers is clearly seen in the energy ranges of 7–15 and 7–22 keV. The S parameter in undoped layers is clearly higher than in the Mg-doped reference sample, indicating positron trapping in vacancy-type defects.

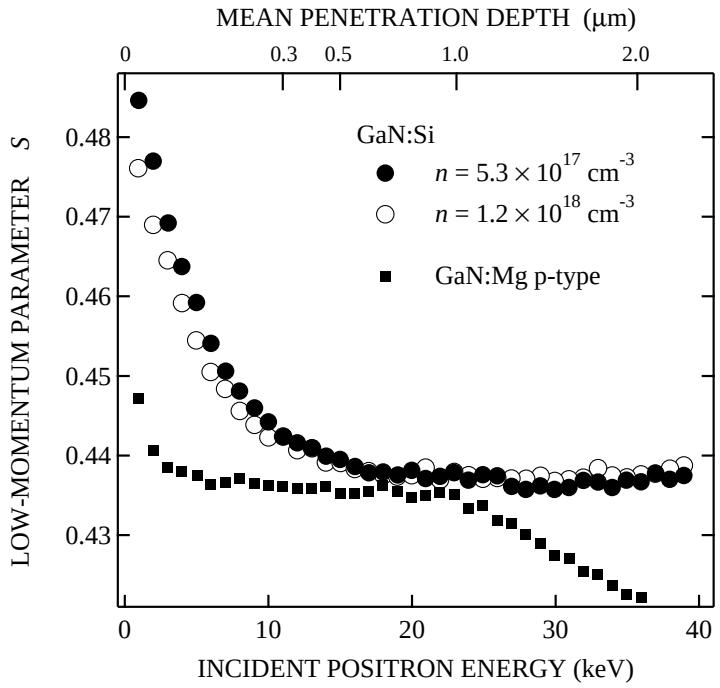

Figure 4: The low-momentum parameter S vs. positron incident energy in two Si-doped GaN layers. The curve measured in p-type GaN layer is shown as a reference level [Publ. II].

The (S,W) points recorded in undoped GaN layers fall on the same line in the S–W plane, indicating that the vacancy is the same in each layer. The slope of the line, which is the fingerprint of the vacancy, is the same as attributed to the Ga vacancy on basis of the positron lifetime experiments in undoped GaN [23] and the investigations of the core electron momentum distribution by two-detector coincidence technique [23, 24]. This leads us to identify the vacancies observed in undoped GaN layers as Ga vacancies.

The effect of the silicon doping on the formation of Ga-vacancies was investigated by studying a set of 3–4 μm thick GaN:Si layers with $n = 5 \times 10^{17} - 5 \times 10^{18}$ cm^{-3}. The doping of GaN with silicon impurities is suggested to suppress the incorporation of residual oxygen. The concentration of Si was shown to be clearly higher than the concentration of residual oxygen impurities by both magneto-optical measurements [25] and SIMS experiments.

The $S(E)$ curves recorded in Si-doped layers (Fig. 4) show that the layer specific S parameter (the plateau at $E > 15$ keV) is very close to the S parameter found in the p-type layers. Similarly, the S parameter does not change significantly as the temperature is increased from 30 to 600 K. In O and Si-doped layers grown in identical conditions the positron experiments show that (i) the O-doping promotes the formation of Ga vacancies and (ii) Si-doped samples have a small V_{Ga} concentration of $\sim 10^{16}$ cm^{-3}.

The observation of the Ga vacancies in n-type nominally undoped layers but not in the p-type and semi-insulating layers coincides with previous investigations [23, 24]. The result agrees with the theoretical calculations [4, 5], which predict that the Ga vacancy has a low formation energy in n-type material.

Interestingly, when the n-type conductivity is due to silicon impurities and less oxygen is present, the Ga vacancies are not observed. This can be explained by the formation of

complexes, such as V_{Ga}– O_N, between Ga vacancies and oxygen, when oxygen impurities are present in the lattice. According to theoretical calculations [5, 7], the formation energy of V_{Ga}– O_N complex is even lower than that of isolated V_{Ga}. The V_{Ga}– O_N complexes may form at the growth temperature when mobile Ga vacancies are trapped by oxygen impurities. In fact, according to a recent study V_{Ga} becomes mobile already at $T \geq 600$ K [26]. Similarly, one could expect the formation of V_{Ga}– Si_{Ga} complexes in Si-doped GaN, as suggested by Kaufmann *et al* [27]. The binding energy of V_{Ga}– O_N pair (1.8 eV) is calculated to be clearly higher than the binding energy of V_{Ga}–Si_{Ga} (0.23 eV) [7], and thus V_{Ga}– O_N pairs are more likely to survive the cool down from the growth temperature. However, the V_{Ga}– Si_{Ga} may be present in some GaN samples [27], particularly since the formation of Ga vacancies is shown to depend also on the stoichiometry of the growth conditions [I]. Unfortunately, the present data cannot distinguish directly between V_{Ga} and V_{Ga}–donor impurity complexes.

3.1.2 Effect of the growth stoichiometry

In addition of the Fermi-level position, also other conditions such as the temperature and the stoichiometry during the growth affect the formation of intrinsic point defects. The effect of the growth stoichiometry on the formation of Ga vacancies in GaN became clearly evident, when we studied a set of MOCVD grown layers where the V/III molar ratio was varied between 1000 and 10000.

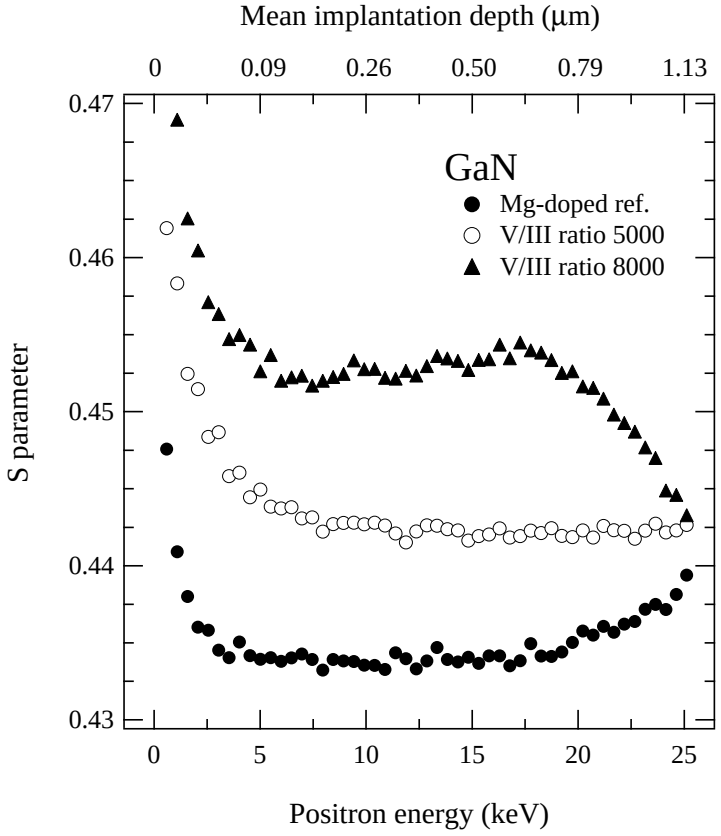

Figure 5: The low momentum parameter S as a function of the positron implantation energy in two layers with different V/III molar ratios [Publ. I].

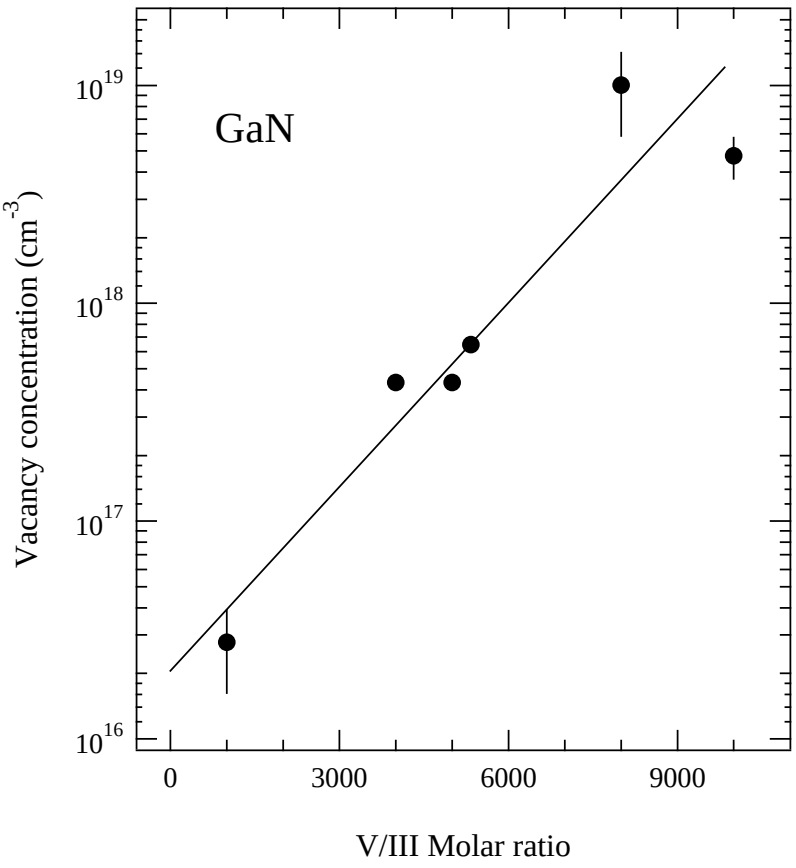

Figure 6: The concentration of Ga vacancies vs. the V/III molar ratio in undoped GaN layers [Publ. I].

The studied layers were 1–5 μm thick epitaxial layers grown on sapphire substrate by MOCVD. By changing the NH_3 flow, the V/III molar ratio was varied between the samples. Although the samples are nominally undoped, they show n-type conductivity with n decreasing from 10^{20} to 10^{16} cm^{-3} as the V/III ratio increases from 1000 to 10000 [28].

The measurement of the Doppler parameters as a function of positron incident energy revealed positron trapping at vacancy-type defects in all layers: The S parameter is clearly higher (Fig. 5) and the W parameter lower in the studied layers than in the p-type GaN:Mg reference sample. In thinner layers the S parameter increases slightly with increasing energy, indicating that the concentration of vacancies is somewhat higher close to the GaN/Al_2O_3 interface.

The observed vacancies are identified by their characteristic slope in the S–W plot. In the S–W plot the points from different layers form a straight line. The slope of the line is the same as found for the Ga vacancies in GaN bulk crystals and epitaxial layers in previous positron studies [23]. Similarly, the core electron momentum distribution, which was measured in the layer with the highest S parameter using two-detector coincidence set-up, was similar to the distribution measured previously for the Ga vacancy.

The vacancy concentrations in the layers were estimated with Eq. (4) and using the estimated value of $S_V/S_b = 1.046$ for the relative vacancy specific S parameter. Interestingly,

the vacancy concentration increases with the increasing V/III molar ratio as shown in Fig. 6. When the growth is conducted in strongly nitrogen rich conditions, a high concentration ($\sim 10^{19}$ cm^{-3}) of empty sites is formed in the Ga sublattice. The result indicates that in addition to the doping and the Fermi-level position discussed above, the formation of the Ga vacancies depends also strongly on the stoichiometry during the growth.

The most probable charge state of the Ga vacancy in n-type GaN is calculated to be -3 and thus it acts as a compensating defect in n-type material [5, 7]. The increase of the vacancy concentration from 10^{16} to 10^{19} cm^{-3} with the increasing V/III molar ratio can thus explain a part of the observed decrease, from 10^{20} to 10^{16} cm^{-3}, in the free electron (Hall) concentration. This suggests that the formation of Ga vacancies has a dominating role in the charge carrier compensation in the studied layers.

As conlusion, the Ga vacancies are observed in n-type GaN, but not in p-type material, reflecting the influence of the Fermi-level position on formation energy of the vacancy. The formation of the Ga vacancies is also strongly affected by the stoichiometry of the growth conditions.

3.2 Vacancy clusters in Si-doped GaN grown by MBE on HVPE GaN template

Molecular-beam epitaxy (MBE) offers a highly controlled way to grow semiconductor epitaxial layers with very low background impurity concentrations. In our study we investigated Si-doped GaN layers (thickness 1.5 μm) grown by MBE on hydride vapor phase epitaxy (HVPE) GaN templates. In the studied samples the template consisted of a 6 μm thick HVPE GaN grown on sapphire substrate. HVPE growth enables a fast growth of thick GaN layers, where the concentrations of impurities and extended defects are reduced. The dislocation density in the templates was $\sim 10^9$ cm^{-2}, an order of magnitude less than close to the GaN/Al_2O_3 interface.

In addition to positron annihilation experiments, the layers were characterized by various other techniques. The electrical properties were measured by Hall and electrochemical capacitance-voltage (ECV) experiments. The optical properties were studied by photoluminescence (PL) experiments. Secondary ion mass spectrometry (SIMS) was used to determine the concentrations of dopant impurities. Although the n-type doping was done with silicon (2×10^{17}– 1×10^{19} cm^{-3}), the SIMS measurements revealed that oxygen was present in concentrations (6×10^{17}–1×10^{18} cm^{-3}). This residual oxygen originates most likely from the GaN/Al_2O_3 interface. The crystal quality and the density of extended defects were determined by transmission electron microscopy (TEM). TEM data showed that the dislocation structures which thread through the HVPE template, are copied also in the MBE layer.

Figure 7 shows the S parameters recorded as a function of positron incident energy. The S parameter in undoped and Si-doped MBE layers is clearly higher than the reference level corresponding to defect-free material (GaN:Mg), indicating that positrons are trapped at vacancy type defects. Interestingly, in the S–W plot (Fig. 8) the (S, W) points do not coincide with the line characteristic to Ga vacancy, indicating that the vacancy in the studied layers is not the same as previously observed in n-type MOCVD layers. The high S parameter value, S/S_b =1.031–1.045, also strongly suggests that the observed vacancy is neither a

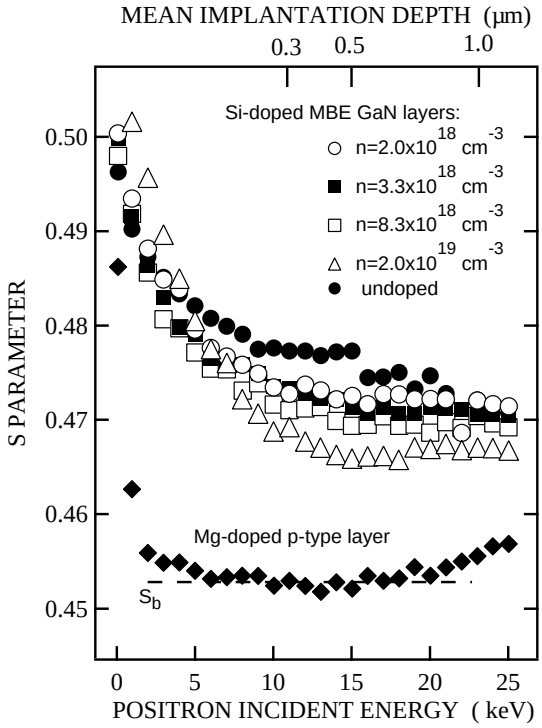

Figure 7: The low momentum parameter S as a function of the positron implantation energy in Si-doped GaN layers grown by MBE [Publ. III].

nitrogen vacancy, which has a much smaller open volume than V_{Ga} and thus should result in clearly lower S values.

The most probable candidate for the observed defect is a vacancy cluster of two or more vacancies. These kind of vacancy clusters have been previously observed in GaN layers grown by MBE on Si(111) substrate [29] and in MOCVD GaN layer grown toward the N face ($[000\overline{1}]$ axis) [30]. The characteristic (S, W) values for the vacancy cluster in Ref. [29] were estimated to be $1.10 \times S_b$ and $0.75 \times W_b$. The measured (S, W) values in Fig. 8 fall close to the line between the GaN lattice point and the point characterizing the vacancy cluster in Ref. [29], suggesting that the defect detected here is the same vacancy cluster as detected in GaN layers on Si(111) substrate.

The measurement of the annihilation parameters as a function of temperature showed that the S parameter increases and the W parameter decreases as the temperature is decreased. This is characteristic of positron trapping at negatively charged vacancies [16]. The increase of the S parameter at low temperatures could also reflect the increase of the positron diffusion length and the associated diffusion-limited positron trapping at the vacancy clusters.

Interestingly, the S parameter and thus the concentration of the clusters decreases as the doping level increases (Fig. 7). An explanation for this can be provided by the presence of also negative Ga monovacancies, or $\mathrm{V_{Ga}}$ related complexes such as $\mathrm{V_{Ga}}$–$\mathrm{O_N}$ or $\mathrm{V_{Ga}}$–$\mathrm{Si_{Ga}}$, in the layers with the highest Si doping level. In Fig. 8 the (S, W) points in the layers with the highest Si doping actually deviate from the line attributed to the cluster, and move towards the line characterizing the Ga vacancy, suggesting that positrons are trapped also

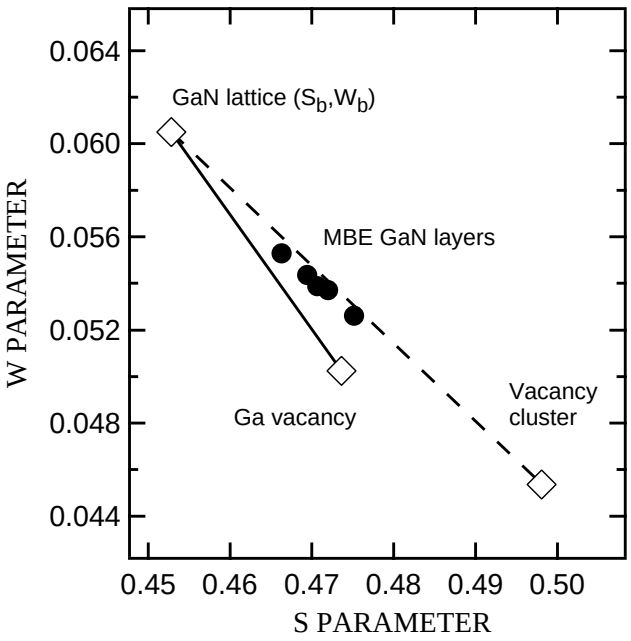

Figure 8: The S–W plot of the MBE GaN layers. (S, W) values specific to defect-free GaN lattice, Ga vacancy, and vacancy cluster are also indicated [Publ. III].

at Ga vacancies.

The emission of parasitic yellow luminescence (YL) is generally related to deep acceptor-type defects [5, 7]. The PL measurements showed that the absolute intensity of yellow luminescence increases with increasing Si-doping, and so it seems improbable that the observed vacancy clusters were involved in the emission of yellow light as their concentration decreases with increasing [Si]. In fact, the vacancy clusters were not found to cause YL in GaN grown on Si(111) [29]. Ga vacancies, on the other hand, have been related to the emission of the YL [23] and thus the change from vacancy clusters to Ga vacancies with increasing [Si] agrees with the PL data.

The microscopic structure of the vacancy clusters and the mechanism leading to their formation cannot unfortunately be solved from the present data. The formation energy of a divacancy V_{Ga}–V_N is calculated to be reduced in n-type material [5], but on the other hand, the positron lifetime experiments in Ref. [30] suggest a defect with a larger open volume than in a divacancy. Interestingly, in Ref. [30] the large volume clusters were detected in the film with N face polarity $(000\overline{1})$. Similarly, in our very recent experiments on O-doped MBE GaN with both N and Ga face polarity, the films grown towards $(000\overline{1})$-direction almost systematically contained vacancy clusters, but they were not observed in the Ga polarity films. In the present study the TEM experiments showed that the crystal had predominately Ga face polarity, but also inversion boundaries were observed. These findings suggest that the formation of vacancy clusters may be related to the growth polarity of the GaN film.

Considering the incorporation of residual oxygen and the density of extended defects, the growth of GaN by the MBE method does not show any significant advantages over vapor phase growth techniques (MOCVD, HVPE), which are much faster and more suitable for large scale production.

3.3 Ga vacancies and the layer structural quality

The growth of high-quality GaN single crystals with reasonable size is difficult and they are not widely available. The GaN material is typically grown epitaxially, most often by MOCVD on sapphire substrate. Due to the large lattice and thermal mismatch between the GaN layer and the sapphire substrate the GaN layers contain typically a high density, 10^8–10^{10} cm^{-2}, of extended defects. Above the interface region the dominating defects are pure edge and mixed screw-edge dislocations which thread through the overlayer up to the surface [31].

Although the operation of GaN devices is surprisingly insensitive to the presence of high dislocation densities, the dislocation lines are shown to be electrically and optically active. The results of electron mobility studies suggest that dislocation lines are negatively charged and contain acceptor states along the line [1, 2]. Cathodoluminescence studies have shown that dislocations act as centers for nonradiative recombination [3], but also evidence of the yellow luminescence emission originating from the dislocation lines has been shown [32].

The microscopic structure of these defects is not fully understood. Different dislocation structures with vacancies in the dislocation core are calculated to be possible, depending on the doping and the stoichiometry during the growth [33]. The edge dislocation with filled-core structure is calculated to be electrically inactive [34], but the observed electrical and optical activity is suggested to result from the Ga vacancies or V_{Ga}-O_N defect complexes which are trapped at the dislocation by the related stress field [35].

3.3.1 Independence of Ga vacancies of dislocation density

In MOVPE growth of GaN on sapphire substrate the increase of the total pressure in the reactor has been found to result in increased grain size and electron mobility [36]. We investigated a set of Si-doped GaN layers [IV], where the average grain size increases from 0.2 to 2–5 μm, as the growth pressure is increased from 39 to 200 Torr. The low-angle grain boundaries are defined by edge dislocations, and they are suggested to be responsible for the low electron mobility and the high degree of compensation observed in lower pressure growths. The major part of the dislocations, > 80 %, are estimated to be located at grain boundaries in the studied layers. We also investigated a nominally undoped GaN layer, which was grown on a Mg-doped bulk GaN crystal [II]. The dislocation density in this homoepitaxially grown sample is very small, close to that in GaN bulk crystals ($< 10^4$ cm^{-2}).

The investigation of homoepitaxially grown undoped GaN layer showed [II] that positrons were trapped at Ga vacancies in the epitaxial overlayer. On the backside of the sample, in the Mg-doped bulk crystal, vacancies were not observed. The presence of the Ga vacancies in the homoepitaxial layer manifests, similarly with the previous results where Ga vacancies have been found in undoped GaN bulk crystals [22, 23], that the dislocations are not required for the formation of the vacancies.

Figure 9 shows the layer characteristic S parameter as a function of temperature in four GaN layers with different grain sizes. In the layer with the smallest grain size, 0.2 μm, the S parameter is the lowest and does not change noticeably with the temperature. This

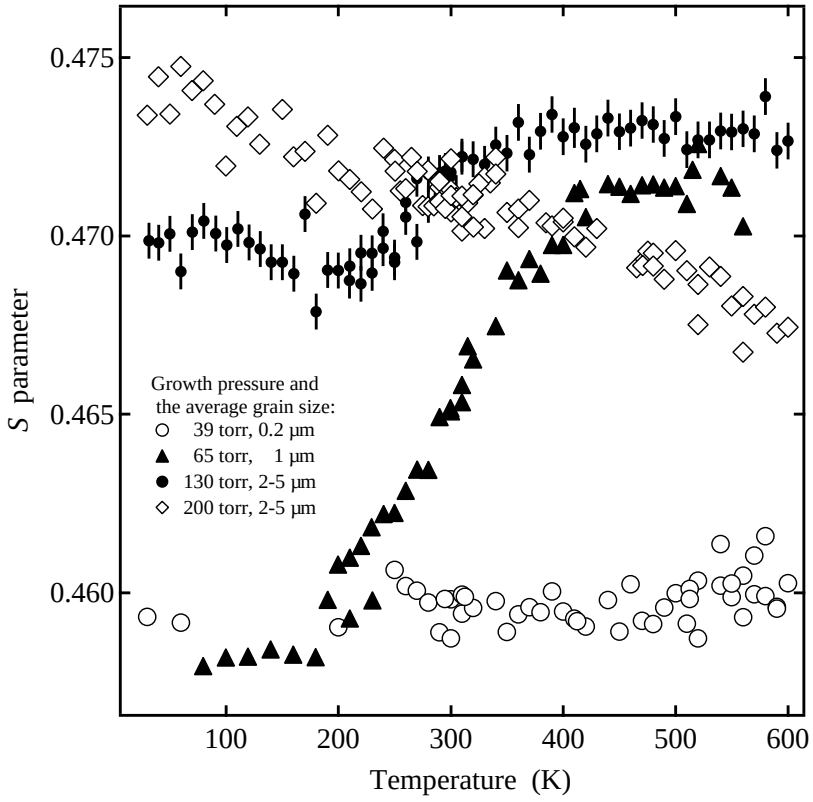

Figure 9: The S parameter vs. measurement temperature in GaN layers with different grain sizes [Publ. IV].

low level is the same as recorded in Mg-doped p-type reference GaN layer and corresponds to the annihilation of positrons in vacancy-free GaN lattice. Thus in the layer with the smallest grain size no positron trapping at vacancies is observed.

In the film grown at the highest pressure, 200 Torr, the S parameter increases with decreasing temperature. This is characteristic of positron trapping at negatively charged vacancies: The positron trapping coefficient μ for direct trapping at negative vacancies varies as $\sim T^{-0.5}$ [16].

In the 65 and 130 Torr films the S parameter is the lowest at low temperatures, $T <$ 200 K, but increases rapidly when the temperature is raised from 200 to 400 K, indicating that the positrons get trapped at vacancies. The decrease in the S parameter at low temperatures is typical of positron trapping into shallow hydrogenic states around negative centers. When these centers do not contain open volume, the corresponding Doppler broadening parameters are similar to those of vacancy-free material. At low temperatures the shallow traps compete with the vacancies in trapping positrons. When the temperature is raised, the escape rate from shallow traps increases rapidly leading to the higher S parameter as more positrons are trapped at vacancies.

The identification of the vacancies is based on the vacancy specific slope in the S–W plot. In the S–W plot the data points measured between 30 K and 600 K fall on the same line in all samples. The slope of the line is the same as found for the Ga vacancy in n-type GaN overlayers and bulk crystals [23]. The result thus indicates that the observed vacancies

are Ga vacancies or complexes involving V_{Ga}.

The concentration of the Ga vacancies can be estimated from the data at high temperature, T > 450 K, where only vacancies act as positron traps. By using the standard trapping model (Eq. 4) and the value 1×10^{15} s^{-1} for the trapping rate μ_V(450K) at Ga vacancies and the ratio S_V/S_b= 1.046 for the vacancy specific S parameter [I], the vacancy concentrations are 5–10$\times 10^{17}$ cm^{-3}.

The observation of Ga vacancies in the higher pressure films is in agreement with previous results, where Ga vacancies were found in n-type samples. In the 39 Torr film which is heavily compensated the vacancies are not observed. The Ga vacancy concentration in the 65, 130, and 200 Torr films varies independently of the average distance between grain boundaries. This suggests that the Ga vacancies are not related to the grain boundaries but are rather located in the grain interior.

3.3.2 Positron trapping at dislocations

The fraction of positrons trapped at shallow traps at low temperatures can be estimated from Fig. 9. In the layer with 1 μm grain size (65 Torr growth) the S parameter drops to the level corresponding to vacancy-free GaN indicating that all positrons get trapped at shallow traps at temperatures below 200 K. In the 130 Torr film the fraction of positrons which get trapped at shallow traps can be estimated using the trapping model of two traps (Eq. 5), where the escape rate δ from the shallow traps is zero at low temperatures. Using the data at 30 K and the value 3.9×10^{15} s^{-1} for μ_V(30 K), the fraction of positrons which annihilate at shallow traps is ∼43 %. In the 200 Torr film the S parameter increases with the decreasing temperature even at low temperatures and there is no clear sign of positron trapping at shallow traps. The S parameter at 30 K is slightly lower than expected if a strict $\sim T^{-0.5}$ behavior for μ_V is assumed, corresponding to max. 10 % contribution of shallow traps. In case of the 39 Torr film the possible existence of shallow traps cannot be observed, because without positron trapping at vacancies the trapping at negative centers, which do not contain open volume, cannot be distinguished from the annihilation of free positrons.

The next question is naturally the origin of these shallow traps. The concentrations of possible acceptor impurities, magnesium and carbon, are measured to be too low to cause the observed compensation of n-type conductivity [37] and the observed positron trapping rate at the shallow traps. The temperature at which positrons escape from the shallow traps ($T > 200$ K) is also higher than previously observed for negative impurities such as Mg [22]. Interestingly, the positron trapping rate at the shallow traps shows clear correlation with the decreasing grain size. This leads us to attribute the negative positron-trapping centers to the edge dislocations located at the grain boundary. Although the total dislocation densities do not vary significantly between the films, the positron diffusion starts to limit the arrival rate at a boundary when the average distance between the boundaries increases. A Monte Carlo simulation of positron diffusion [38] gives estimates 85 %, 25 %, 12 % and, 4 % for the fraction of positrons which could reach the boundary in 0.2 μm, 1μm, 2 μm, and 5 μm grains, respectively. Although these fractions are clearly below the experimental fractions of positrons trapped at grain boundaries, they reflect the same ratios and range as the experimental ones. In reality the dislocations located inside the grains, the straggling of the grain boundaries, and the electrostatic attraction of the dislocations increase the possibility

of positron to reach a dislocation.

As a summary, the presence of the Ga vancancies in the low dislocation density material and the independence of vacancy concentrations of the average grain size shows that the formation of V_{Ga} is not related to the dislocations. The positron data suggests that the edge dislocations are negatively charged and they do not contain open volume. The suggested negative charge of the edge dislocation is consistent with cathodoluminescence [3, 32] and mobility studies [1, 2]. Similarly, the result agrees with Z-contrast imaging studies [39], where no evidence of high concentrations of Ga vacancies was found, and thus disagrees with the calculations which predict the existence of Ga vacancies in the dislocation structure [33, 35].

4 Native vacancies in nitrogen doped and undoped ZnSe layers

Fundamental problems exist in fabrication of device-quality ZnSe. Doping into p-type is difficult due to strong compensation of acceptor impurities. The material also degrades during the operation, which is related to the formation of point and extended defects.

The most important native defect in n-type ZnSe is calculated to be the zinc vacancy [40], which has been studied in detail by electron paramagnetic resonance and ODMR experiments in electron irradiated n-type ZnSe [41]. Zinc vacancies have been detected also in positron annihilation experiments in n-type materials, in Cl-doped $ZnS_{0.06}Se_{0.94}$ and in I- and Ga-doped ZnSe [42, 43, 44, 45]. In positron experiments p-type N-doped $ZnS_{0.06}Se_{0.94}$ layers have been found to contain selenium vacancies, which are probably paired with N impurities [42]. Undoped ZnSe layers have often been considered as defect-free [43, 44, 45].

4.1 Se vacancies in N-doped layers

In our work [V] we studied N-doped and undoped ZnSe layers grown by MBE on GaAs:Si substrate. As reference samples without lattice mismatch we studied a homoepitaxial undoped ZnSe layer, grown on Se-rich ZnSe crystal, and an undoped ZnSe bulk crystal grown in Zn-rich conditions.

The N-doped ZnSe layers, BN1, BN2, and BN3 were $\sim$3 μm thick. The N impurity concentrations were (8–10)$\times 10^{16}$, (5–10)$\times 10^{17}$, and (8–15)$\times 10^{18}$ cm^{-3} in BN1, BN2, and BN3, respectively. The S–W plot in Fig. 10 shows the annihilation parameters characterizing each N-doped layer, together with the parameters recorded in I-doped sample (MI). The (S, W) points in N-doped layers fall in the same line, indicating positron trapping at a single type of vacancy. In Fig. 10 the vacancy concentration increases with the N impurity concentration. The S parameter is the lowest in sample BN1, indicating that the vacancy concentration is the lowest in this sample. In fact, the Doppler parameters recorded at room temperature in BN1 are practically the same as found in the Zn rich undoped bulk ZnSe crystal. The positron lifetime measurement in this sample gives a single lifetime of 239 ± 1 ps, which coincides with the theoretical value of 240 ps for annihilation in defect-free ZnSe lattice [46]. Thus the room-temperature annihilation parameters in the sample BN1 correspond to positron annihilation in vacancy-free ZnSe lattice. However, the behavior of the annihilation parameters as a function of temperature suggests a small concentration of vacancies (discussed in section 4.3) also in BN1.

The vacancy in N-doped layers is characterized by the slope $R_V = |\Delta S|/|\Delta W| \approx 4.8$. Saarinen *et al.* [42] found N-doped $ZnS_{0.06}Se_{0.94}$ layers to contain vacancies, which were identified as Se vacancies by the shape of the high momentum part of the annihilation spectrum and were characterized by the slope $R_{V_{\mathrm{Se}}} \approx 5$. Therefore, we associate the line with the slope $R_V \approx 4.8$ to the selenium vacancy in ZnSe.

The charge state of an isolated selenium vacancy is calculated to be 2+ in ZnSe [10, 40]. Since positive vacancies do not trap positrons, the detected selenium vacancy must be a part of a complex with a neutral or negative total charge. Theoretical calculations predict that in N-doped ZnSe the most abundant complex containing a Se vacancy–

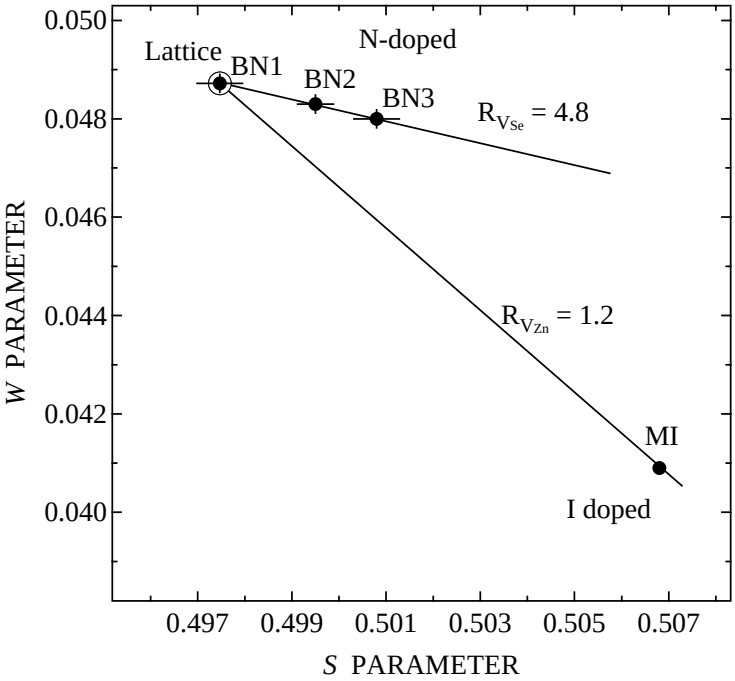

Figure 10: The (S, W) values characteristic of the N-doped and I doped ZnSe layers [Publ. V].

nitrogen impurity pair [10, 40]. This leads us to attribute the detected vacancies in N-doped samples as V_{Se}-N_{Se} complexes.

4.2 Zn vacancies in undoped layers

The line between n-type I-doped sample MI and the lattice point has a clearly different slope, $R_V \approx 1.2 - 1.6$, indicating positron trapping at another kind of vacancies in this sample. The lower R parameter means that less annihilations take place with core electrons than in the case V_{Se}. This indicates that the vacancy in I-doped layer is V_{Zn}, because the 3d electrons of the Se atoms surrounding the zinc vacancy overlap much less with the positron wave function than those of Zn atoms neighboring V_{Se} [42].

In the studied undoped ZnSe layers the layer thickness and structural quality varies: In three thin layers (BUd_1, BUd_2, and BUd_3) with the layer thickness <1.5 μm the dislocation densities measured by etch pit density and by TEM were 10^6, 1–2$\times 10^7$, and 10^9–10^{10} cm^{-2}, respectively. In the 4.2 μm thick layer BU and in the homoepitaxial layer HU the structural quality should be clearly better.

The representative S and W parameters for undoped ZnSe layers (Fig. 11) fall clearly apart from the lattice point and are consistent with the line $R \approx 1.2 - 1.6$ attributed to V_{Zn}. This indicates that zinc vacancies are present in all studied undoped samples.

The measurement of the annihilation parameters as a function of temperature shows that the S parameter increases and the W parameter decreases as the temperature is decreased [V]. This behavior is characteristic of positron trapping at negative vacancies [16, 17], indicating that the observed zinc vacancies are in a negative charge state. The data show no evidence of positron trapping at other defects, such as shallow traps at low temperatures. The observed negative charge state agrees with the theoretical calculations [40] which pre-

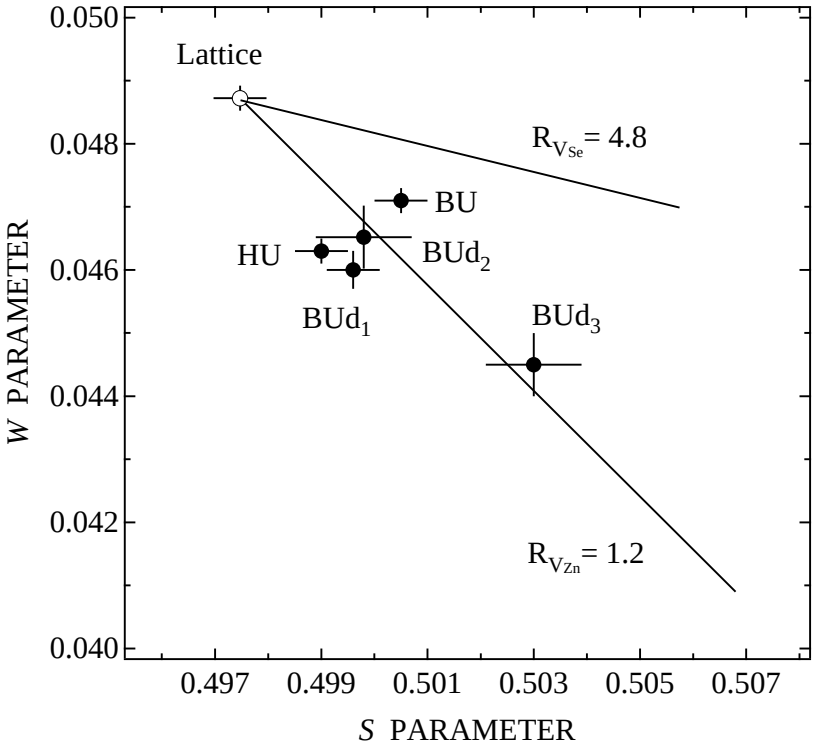

Figure 11: The (S, W) values characteristic of the undoped ZnSe layers. The wider error bars in thin BUd samples represent the uncertainties due to graphical extrapolation. The lines corresponding to Se and Zn vacancies are also shown [Publ. V].

dict that in undoped ZnSe the most probable negative native defect is the Zn vacancy in the doubly negative charge state. The absence of positron trapping at negative ions also agrees with theoretical calculations [47, 40], which predict that the intrinsic negative ions, such as Zn_{Se} antisite defects, have a very high formation energy in undoped ZnSe.

The concentration of zinc vacancies is roughly the same, 2–4$\times 10^{16}$ cm^{-3} in the homoepitaxial sample HU, in the thick heteroepitaxial sample BU, and in the thin layers BUd$_1$ and BUd$_2$ with lower dislocation densities. In the layer BUd$_3$ with the highest dislocation density, 10^9–10^{10} cm^{-2}, also the concentration of zinc vacancies is the highest, $\sim 10^{17}$ cm^{-3}. The result thus suggests that in addition to doping and its influence on the defect formation energy, the creation of zinc vacancies is also somewhat enhanced by the lattice mismatch between ZnSe layer and GaAs substrate.

4.3 Compensation of p-type doping in $ZnS_{0.06}Se_{0.94}$ and ZnSe

The p-type doping of ZnSe has proven to be difficult. The best results are obtained with nitrogen impurities. The charge carrier concentrations have been found, however, to saturate at about $\leq 10^{18}$ cm^{-3} regardless of much larger amount of incorporated nitrogen atoms. It has been proposed that the deactivation of acceptors could be caused by the formation of dopant impurity–native defect pairs [10]. In N-doped ZnSe the formation of defect complexes involving a substitutional nitrogen dopant with a selenium vacancy V_{Se} or a zinc interstitial Zn_i is calculated to be energetically favored [40]. Also the creation of N_2

molecules [11] and dopant atom related lattice instability which turns a shallow acceptor level into a deep one [12], are suggested.

We have studied the deactivation of nitrogen doping in detail in 1.5–2.0 μm thick $ZnS_{0.06}Se_{0.94}$ layers [VI]. The alloying with Zn enables a good lattice match with the GaAs substrate resulting in good quality epitaxial film. The layers were grown on GaAs(100) substrate by two different MBE systems (sets A and B). The concentration of N impurities was determined by SIMS, and the resulting hole concentrations were measured by electrochemical capacitance-voltage (CV) experiments. The results (Table I) show that $p \ll$ [N] in every sample, indicating strong deactivation of impurities.

The Doppler parameters S and W characterizing each layer were measured using low energy positron beam. Figure 12 shows the S parameter values in various layers measured at a positron energy of 10 keV at 25–500 K. With this energy all positrons annihilate inside the $ZnS_{0.06}Se_{0.94}$ overlayer and do not diffuse to the sample surface or to the substrate. The S parameter values in Fig. 12 are scaled with S_b, the S parameter corresponding to positron annihilation in defect-free $ZnS_{0.06}Se_{0.94}$, taken from Ref. [42].

At temperatures $T > 200$ K the S parameter is clearly higher than S_b in all samples, indicating that positrons get trapped at vacancy type defects. These vacancies have been identified as Se vacancies by the shape of the core electron momentum distribution [42]. The charge state of an isolated Se vacancy is expected to be 2+ [10] and thus it is repulsive to positrons. Therefore the detected Se vacancy is most likely a part of a defect complex, most probably with the N impurity [40], so that the total charge of the defect is negative or neutral.

The S parameter decreases in all layers when the temperature is lowered, indicating a smaller fraction of annihilations at vacancies (Fig. 12). This can be explained by positron trapping into Rydberg states around negative ions at low temperatures. At low temperatures these shallow traps compete with vacancies in trapping positrons. As the surroundings of

Table I: The charge carrier and the N impurity concentrations from CV and SIMS measurements and the concentrations of negative vacancies and negative ions from the positron annihilation experiments.

Sample	p (cm^{-3})	[N] (cm^{-3})	c_V (cm^{-3})	c_{ion} (cm^{-3})
Set A:				
1	1.0×10^{17}	2.9×10^{19}	4.0×10^{18}	1.1×10^{19}
2	2.6×10^{17}	1.5×10^{18}	2.9×10^{17}	3.1×10^{17}
3	3.5×10^{17}	4.8×10^{18}	3.9×10^{17}	2.9×10^{18}
4	2.4×10^{17}	1.1×10^{18}	2.9×10^{17}	4.2×10^{17}
5	2.0×10^{17}	2.0×10^{18}	2.9×10^{17}	4.9×10^{17}
Set B:				
6	3.5×10^{17}	3.8×10^{18}	3.0×10^{17}	2.4×10^{17}
7	2.0×10^{17}	5.1×10^{18}	2.4×10^{17}	2.8×10^{17}
8	4.0×10^{17}	4.1×10^{18}	2.6×10^{17}	2.6×10^{17}
9	2.8×10^{17}	3.4×10^{18}	2.6×10^{17}	2.6×10^{17}

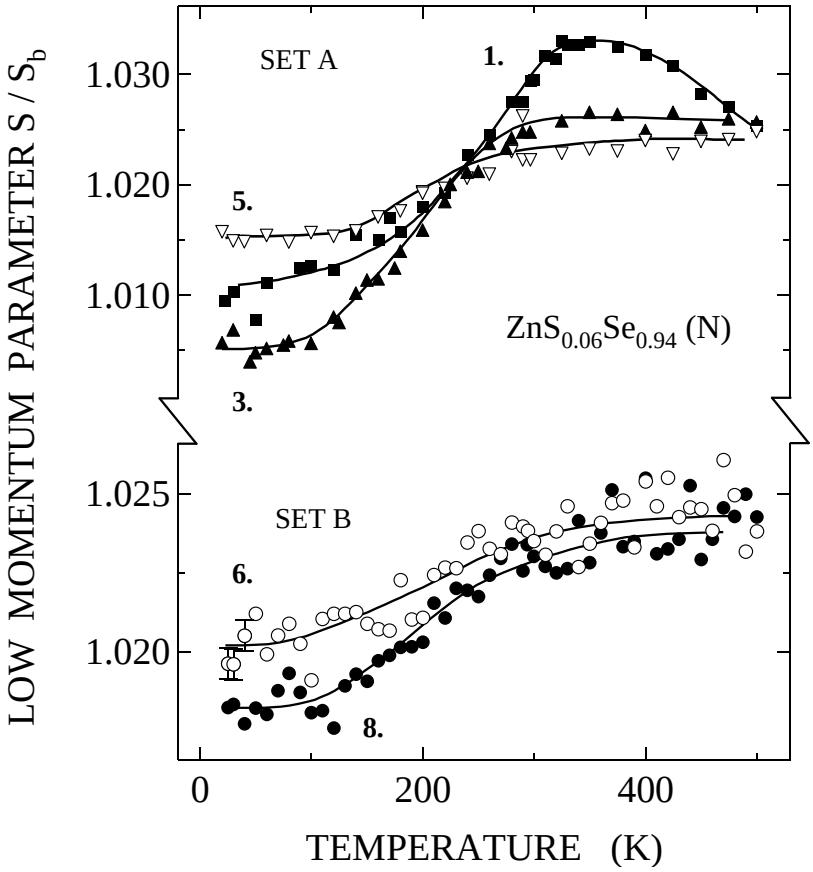

Figure 12: The low momentum parameter S/S_b vs. measurement temperature in various $ZnS_{0.06}Se_{0.94}$:N samples. The sample numbers, corresponding to Table I, are indicated in the figure. The solid lines are guides to the eye [Publ. VI].

negative ions do not contain any open volume, the S parameter decreases towards the bulk value S_b.

The charge state of the V_{Se}-N_{Se} can be determined on basis of Fig. 12. At temperatures below 100 K the S parameter is constant as a function of temperature. The positron trapping coefficients at negative ions and negative vacancies both behave as $\sim T^{-1/2}$, whereas the trapping at neutral vacancies is independent of temperature [16, 48]. If neutral vacancies and negative ions were competing as positron traps, the S parameter would decrease when temperature is lowered. The observed V_{Se}-N_{Se} complexes must thus be negatively charged, to cancel the temperature behavior of positron trapping at negative ions.

The concentrations of the V_{Se}-N_{Se} complexes and the negative ions were estimated from the positron data. At high temperatures $T > 300$ K positrons are not trapped at negative ions. The measured S parameter is then a linear combination of the values characteristic to the annihilations in the lattice (S_b) and at the vacancies (S_V) only and the vacancy concentration can be estimated by Eq. (4). At lower temperatures (<50 K) the S parameter is a superposition of the values S_b, S_V and that obtained at negative ions $S_{ion} \approx S_b$. At 25 K we can assume that the detrapping rate δ from the ions is zero and estimate the concentration of negative ions using Eq. (5).

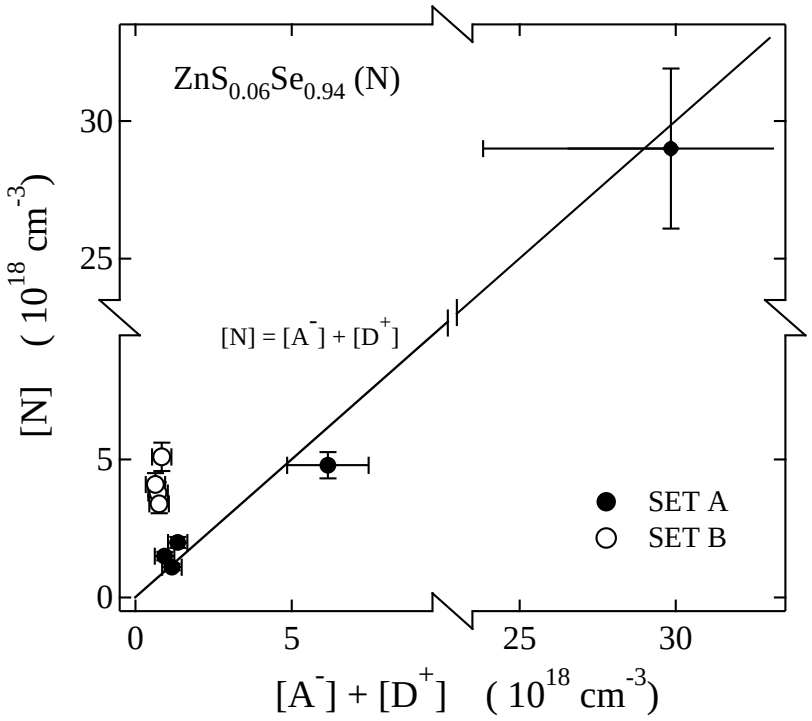

Figure 13: The concentration of incorporated nitrogen atoms as a function of the sum of donor and acceptor concentrations. The samples of set A are indicated by black circles and the samples of set B by white circles. The line $[N] = [A^-] + [D^+]$ is shown in the figure [Publ. VI].

The concentrations of negative V_{Se}-N_{Se} complexes and negative ions (Table I) represent the total concentration of acceptor type defects, $[A^-] = c_V + c_{ion}$ in each sample. The concentration of donor type defects $[D^+]$ can thus be calculated from the hole concentration $p = [A^-] - [D^+]$ measured by CV.

Figure 13 shows the concentration of incorporated nitrogen $[N]$ obtained by SIMS as a function of the sum of acceptor and donor concentrations, $[A^-] + [D^+]$. As mentioned above, the theoretical calculations predict that the most probable defects in N-doped ZnSe are those related to nitrogen impurities. The samples from the set A obey quite well the correlation $[N] = [A^-] + [D^+]$, suggesting that in the set A all nitrogen atoms are related to charged defects. In the samples of the set B that correlation does not hold, indicating that these samples contain N atoms also in electrically neutral form.

The most obvious candidate for the negative ion is the N_{Se} acceptor. According to calculations [40], the most likely assignment of the donor defect is either $(Zn_i\text{-}N_{Se})^{1+}$ or $(V_{Se}\text{-}N_{Se})^{1+}$. In set A the concentration of charged defects increases linearly with the nitrogen incorporation (Fig. 14). About 40 % of all nitrogen impurities are situated as isolated acceptors N_{Se}^-. Another ∼40 % is in donor type defect pairs $(Zn_i\text{-}N_{Se})^{1+}$ or $(V_{Se}\text{-}N_{Se})^{1+}$ and about 20 % is bound to the negative $(V_{Se}\text{-}N_{Se})^{1-}$ pairs.

In the sample set B the situation is totally different. The major part, ∼80 %, of the incorporated nitrogen is in electrically neutral form. Unfortunately the location of the nitrogen impurities can not be concluded with the present data. The existence of defect

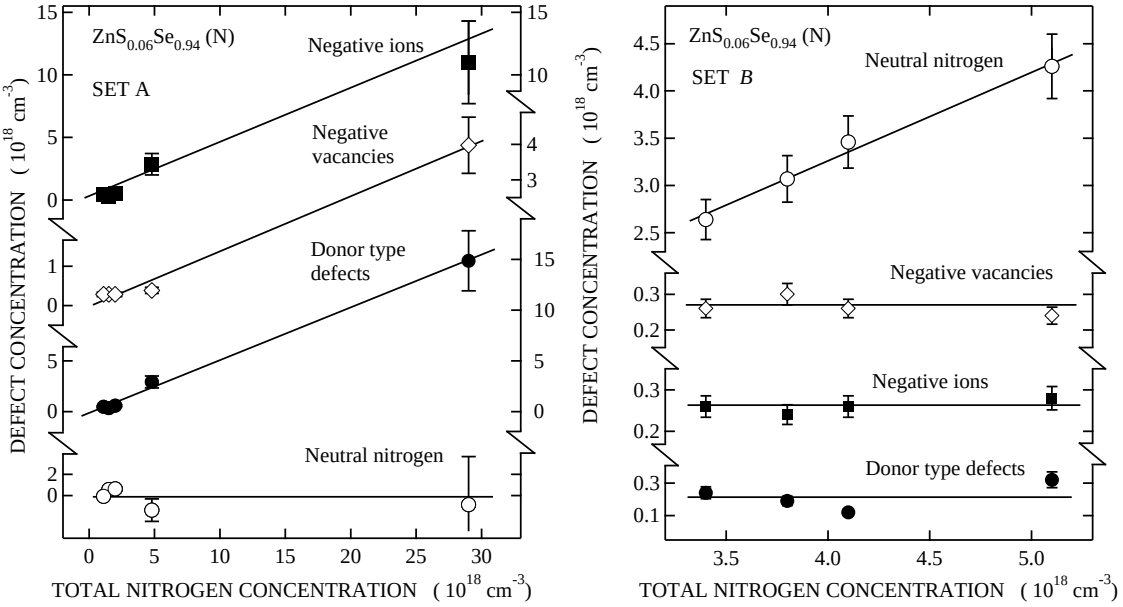

Figure 14: The estimated defect concentrations as a function of the total concentration of incorporated nitrogen in the samples of set A (left) and B (right) [Publ. VI][49].

complexes Zn_i-N_{Se} or V_{Se}-N_{Se} in neutral charge state is not likely according to theoretical calculations [40]. One possibility is the formation of neutral N–N complexes, which are suggested by theory [11] and by an ion beam analysis on N-doped ZnSe [50].

The results suggest that the observed deactivation of nitrogen impurities in $ZnS_{0.06}Se_{0.94}$ may result from two different mechanisms; by the formation of compensating donor type defects or by the introduction of neutral nitrogen related complexes. The differences between the two sets of samples suggest that the details of the MBE growth system and the growth conditions may have a strong influence on the activation of nitrogen. In our case the difference between the two sets may be due to the slightly different growth stoichiometry.

The analysis of the positron annihilation data in N-doped ZnSe layers BN1, BN2, and BN3 gave very similar results as above [V]. The layer specific S parameter increases with increasing temperature in each layer (Fig. 15). The S parameter observed at $T > 200$ K is due to positron trapping at vacancy-type defects, identified as V_{Se}-N_{Se} complexes (Sec. 4.1). In BN1 the S parameter increases slightly at temperatures $T < 200$ K. Between $T \approx 200$ K and $T \approx 350$ K the increase is steeper, until at $T < 350$ K the S parameter turns to an almost constant level. The total increase, $\sim$0.16%/100 K, in this sample is comparable with the increase 0.12%/100 K observed in defect-free GaAs [51] and can be attributed almost entirely to the thermal expansion of the lattice. In samples BN2 and BN3 the S parameter at low temperatures ($T < 200$ K) is at about the same level as in BN1, but increases then rapidly with the temperature. The rapid increase in the S parameter indicates that positrons are trapped at low temperatures into shallow Rydberg states around negative ions, which in N-doped ZnSe are most likely N_{Se} acceptors. As the temperature is increased, positrons escape the negative ions and the larger value of S parameter due to trapping at vacancies is restored.

Interestingly, above 350 K the S parameter starts to decrease in both BN2 and BN3

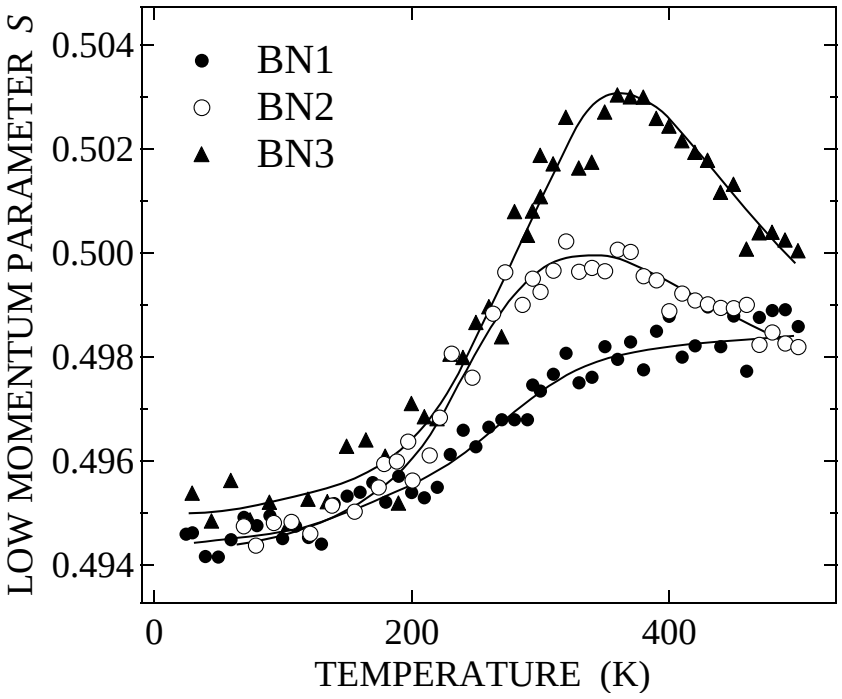

Figure 15: The low momentum parameter S vs. measurement temperature in N-doped ZnSe layers [Publ. V].

samples. The $\sim T^{-1/2}$ behavior of the positron trapping coefficient expected for negative vacancies [16, 48] explains only part of the decrease in S. A similar decrease in the S parameter can be also seen in Fig. 12 in the heavily compensated sample #1 and it has been observed also in N-doped $Mg_yZn_{y-1}S_xSe_{x-1}$ layers [49]. The observed decrease in the S parameter is most likely due to charge state change of the V_{Se}-N_{Se} vacancy complex. When Fermi level reaches the ionization level of the V_{Se}-N_{Se} in the band gap, the vacancy complex is converted into more negative charge state. If the charge state change is accompanied by a lattice relaxation inwards, the S parameter decreases as seen in Figs. 12 and 15.

Similarly to ZnSSe layers, the data in Fig. 15 is used to estimate the concentrations of V_{Se}-N_{Se} complexes and N_{Se}^{-1} acceptors. At temperature T ~350 K, where the S parameter reaches the maximum, the trapping into negative ions has very small effect and thus we can make a lower limit estimate for the concentration of vacancies using the data at 350 K and the standard positron trapping model (Eq. 4). Using the value $S_V/S_b = 1.035$ and S_b=0.497 for the lower limit estimate, the vacancy concentrations in the heavily doped samples BN2 and BN3 are $(3 \pm 1) \times 10^{16}$ cm^{-3} and $(6 \pm 2) \times 10^{16}$ cm^{-3}. In sample BN1 the temperature behavior of the annihilation parameters suggests that it may contain some vacancies, even if the S parameter at 300 K is close to the estimated S_b. The vacancy concentration is however very small, below 10^{16} cm^{-3}. At low temperatures, where the S parameter is a superposition of values S_b, S_V, and $S_{ion} = S_b$, the S parameter strongly approaches the bulk value in all layers. Therefore it is possible to only give lower limit estimates (Table II) for the concentration of negative ions.

The total concentration acceptor-type defects (Table II) in heavily doped samples is higher than the net acceptor concentration given by CV measurement, suggesting that donor-

Table II: The concentrations of observed selenium vacancy complexes and negative ions in N-doped ZnSe samples. The samples were grown by MBE on GaAs:Si substrate and the net acceptor concentration was determined by capacitance-voltage measurements [V].

Sample	[N] (cm^{-3})	Net acceptor concentration N_a-N_d (cm^{-3})	Layer thickness (μm)	Se vacancy concentration (cm^{-3})	Negative ions (cm^{-3})
BN1	$(8-10)\times10^{16}$	$(2-5)\times10^{16}$	3	$<10^{16}$	–
BN2	$(5-10)\times10^{17}$	$(3-6)\times10^{17}$	2.8	$(3\pm1)\times10^{16}$	$(4-8)\times10^{17}$
BN3	$(8-15)\times10^{18}$	$(1-4)\times10^{17}$	3.1	$(6\pm2)\times10^{16}$	$(1-2)\times10^{18}$

type compensating defects must be present in noticeable concentrations. As the concentration of incorporated nitrogen is clearly higher than the concentration of acceptor type defects, it is natural to think that a large fraction of nitrogen impurities are situated also in donor-type defects, leading to electrical deactivation. Although the data in N-doped ZnSe do not allow an exact quantitative analysis, the results show that the electrical compensation is due to high concentration of donor type defects as found above in the $ZnS_{0.06}Se_{0.94}$ samples of the set A.

5 Summary

In this work, the influence of doping and layer structural quality to point defects in GaN and ZnSe compound semiconductor layers have been studied by positron annihilation spectroscopy. The measurements have been done using a low-energy positron beam, which enables the depth scanning of few micrometer thick overlayers.

Ga vacancies were found in high concentrations in undoped n-type GaN layers, where the n-type conductivity is due to residual oxygen impurities. Being negatively charged, the Ga vacancies constituted the major compensating defect in these layers. In p-type and in semi-insulating Mg-doped layers the Ga vacancies were not observed. In samples where the n-type conductivity is achieved by silicon doping, however, clearly less gallium vacancies were observed than in samples containing oxygen, suggesting that the presence of oxygen leads to the formation of stable gallium vacancies complexed with oxygen impurities. The observation is in good agreement with theoretical calculations predicting low formation energy and high binding energy for V_{Ga}-O_N complex in n-type GaN [7, 5].

In addition to doping, the formation of Ga vacancies was found to depend strongly on the stoichiometry of the growth conditions. The formation of Ga vacancies showed, however, no obvious dependence on the layer structural quality. Ga vacancies were observed as well in homoepitaxially grown material, where the dislocation density is greatly reduced, as in the layers grown on sapphire substrate. In layers with different grain sizes, no dependence between the concentration of Ga vacancies and the grain size was seen. Positrons were found to get trapped at shallow traps around negative centers, which were attributed to the edge dislocations. The result indicates that the edge dislocations are negatively charged, but they do not contain vacancy type defects.

Si-doped GaN layers grown by molecular-beam epitaxy were found to contain negatively charged vacancy clusters, with open volume greater than that of a monovacancy. The concentration of the clusters decreased with increasing silicon doping. However, also evidence of Ga monovacancies was obtained.

In nitrogen doped ZnSe and $ZnS_{0.06}Se_{0.94}$ layers positron trapping at vacancies and negative ions was observed. The vacancies were assigned as V_{Se}-N_{Se} complexes and the negative ions as isolated N_{Se} acceptors. By relating the concentrations of these acceptor-type defects to the net charge carrier concentration given by capacitance-voltage measurements and to the total nitrogen concentration measured by secondary ion mass spectrometry, both qualitative and quantitative information on the deactivation of N impurities was obtained. The data suggested that the deactivation can take place by two different mechanisms; by the formation of compensating nitrogen related donor defects, most likely $(Zn_i$-$N_{Se})^+$ or $(V_{Se}$-$N_{Se})^+$, and by the incorporation of nitrogen in electrically neutral form, e.g. as neutral N–N complexes.

In undoped ZnSe samples negative zinc vacancies were observed at concentrations of 10^{16}–10^{17} cm^{-3}. No clear difference in vacancy concentration was found between homoepitaxial layer and heteroepitaxial layers with low dislocation densities ($\leq 2 \times 10^7$ cm^{-2}) at ZnSe/GaAs interface. In the sample with high dislocation density, 10^9–10^{10} cm^{-2}, also the concentration of Zn vacancies was slightly higher, suggesting that the presence of extended defects in the ZnSe lattice may have an influence on the formation of point defects such as the Zn vacancy.

References

1 N. G. Weinman, L. F. Eastman, D. Doppalapudi, H. M. Ng, and T. D. Moustakas, J. Appl. Phys. **83**, 3656 (1998).

2 D. C. Look and J. R. Sizelove, Phys. Rev. Lett. **82**, 1237 (1999).

3 S. J. Rosner, E. C. Carr, M. J. Ludowise, G. Girolami, and H. I. Erikson, Appl. Phys. Lett. **70**, 420 (1997).

4 J. Neugebauer and C. G. Van de Walle, Phys. Rev. B **50**, 8067 (1994).

5 T. Mattila and R. M. Nieminen, Phys. Rev. B **55**, 9571 (1997).

6 G.-C. Yi and B. W. Wessels, Appl. Phys. Lett. **69**, 3028 (1996).

7 J. Neugebauer and C. G. Van de Walle, Appl. Phys. Lett. **69**, 503 (1996).

8 D. C. Look, D. C. Reynolds, J. W. Hemsky, J. R. Sizelove, R. L. Jones, and R. J. Molnar, Phys. Rev. Lett. **79**, 2273 (1997).

9 J. Neugebauer and C. G. Van de Walle, in *Gallium Nitride and Related Materials*, Vol. 395 of *MRS Symposia Proceedings*, edited by F. A. Ponce, R. D. Dupuis, S. Nakamura, and J. A. Edmond (Materials Research Society, Pittsburg, 1996), p. 645.

10 A. Garcia and J. E. Northrup, Phys. Rev. Lett. **74**, 1131 (1995).

11 B.-H. Cheong, C. H. Park, and K. J. Chang, Phys. Rev. B **51**, 10610 (1995).

12 C. H. Park and D. J. Chadi, Phys. Rev. Lett. **75**, 1134 (1995).

13 G. C. Hua, N. Otsuka, D. C. Grillo, Y. Fan, J. Han, M. D. Ringle, R. L. Gunshor, M. Hovinen, and A. Nurmikko, Appl. Phys. Lett. **65**, 1331 (1994).

14 S. Gundel, D. Albert, J. Nürnberger, and W. Faschinger, Phys. Rev. B Rapid Communications **60**, 16271 (1999).

15 P. J. Schultz and K. G. Lynn, Rev. Mod. Phys. **60**, 701 (1988).

16 K. Saarinen, P. Hautojärvi, and C. Corbel, in *Identification of defects in semiconductors*, edited by M. Stavola (Academic Press, New York, 1998), p. 209.

17 R. Krause-Rehberg and H. S. Leipner, *Positron annihilation in semiconductors* (Springer-Verlag, Berlin, 1999).

18 M. J. Puska and R. M. Nieminen, Rev. Mod. Phys. **66**, 841 (1994).

19 S. Mantl and W. Triftshäuser, Phys. Rev. B **27**, 1645 (1978).

20 M. Alatalo, H. Kauppinen, K. Saarinen, M. J. Puska, J. Mäkinen, P. Hautojärvi, and R. M. Nieminen, Phys. Rev. B **51**, 4176 (1995).

21 C. Wetzel, T. Suski, J. W. Ager III, E. R. Weber, E. E. Haller, S. Fischer, B. K. Meyer, and R. J. Molnar, Phys. Rev. Lett. **78**, 3923 (1997).

22 K. Saarinen, J. Nissilä, P. Hautojärvi, J. Likonen, T. Suski, I. Grzegory, B. Lucznik, and S. Porowski, Appl. Phys. Lett. **75**, 2441 (1999).

23 K. Saarinen, T. Laine, S. Kuisma, J. Nissilä, P. Hautojärvi, L. Dobrzynski, J. M. Baranowski, K. Pakula, R. Stepniewski, M. Wojdak, A. Wysmolek, T. Suski, M. Leszczynski, I. Grzegory, and S. Porowski, Phys. Rev. Lett. **79**, 3030 (1997).

24 L. V. Jorgensen, A. C. Kruseman, H. Schut, A. V. Veen, M. Fanciulli, and T. D. Moustakas, in *Gallium Nitride and Related Materials*, Vol. 449 of *MRS Symposia Proceedings*, edited by F. A. Ponce, T. D. Moustakas, I. Akasaki, and B. A. Monemar (Materials Research Society, Pittsburg, 1997), p. 853.

25 A. M. Witowski, M. L. Sadowski, K. Pakula, B. Suchanec, R. Stepniewski, J. M. Baranowski, M. Potemski, G. Martinez, and P. Wyder, MRS Internet J. Nitride Semicond. Res. **3**, 33 (1998).

26 K. Saarinen, T. Suski, I. Grzegory, and D. C. Look, Phys. Rev. B **64**, 233201 (2001).

27 U. Kaufmann, M. Kunzer, O. Obloh, M. Maier, C. Manz, A. Ramakrishnan, and B. Santic, Phys. Rev. B **59**, 5561 (1999).

28 O. Briot, J. P. Alexis, S. Sanchez, B. Gil, and R. L. Aulombard, Solid-State Electron. **41**, 315 (1997).

29 E. Calleja, M. A. Sánchez-Garcia, D. Basak, F. J. Sánchez, F. Calle, P. Youinou, E. Muñoz, J. J. Serrano, J. M. Blanco, C. Villar, T. Laine, J. Oila, K. Saarinen, P. Hautojärvi, C. H. Molloy, D. J. Somerford, and I. Harrison, Phys. Rev. B **58**, 1550 (1998).

30 A. Uedono, S. F. Chichibu, Z. Q. Chen, M. Sumiya, R. Suzuki, T. Ohdaira, T. Mikado, T. Mukai, and S. Nakamura, J. Appl. Phys. **90**, 181 (2001).

31 X. H. Wu, L. M. Brown, D. Kapolnek, S. Keller, B. Keller, S. P. DenBaars, and J. S. Speck, J. Appl. Phys. **80**, 3228 (1996).

32 F. A. Ponce, D. P. Bour, W. Götz, and P. J. Wright, Appl. Phys. Lett. **68**, 57 (1996).

33 A. F. Wright and U. Grossner, Appl. Phys. Lett. **73**, 2751 (1998).

34 J. Elsner, R. Jones, P. K. Sitch, V. D. Porezag, M. Elstner, Th. Frauenheim, M. I. Heggie, S. Öberg, and P. R. Briddon, Phys. Rev. Lett. **79**, 3672 (1997).

35 J. Elsner, R. Jones, M. I. Heggie, P. K. Sitch, M. Haugk, T. Frauenheim, S. Öberg, and P. R. Briddon, Phys. Rev. B **58**, 12571 (1998).

36 D. D. Koleske, A. E. Wickenden, R. L. Henry, M. E. Twigg, J. C. Culbertson, and R. J. Gorman, Appl. Phys. Lett. **73**, 2018 (1998).

37 A. E. Wickenden, D. D. Koleske, R. L. Henry, R. J. Gorman, M. E. Twigg, M. Fatemi, J. A. Freitas, Jr., and W. J. Moore, J. Electron. Mater. **29**, 21 (2000).

38 C. Hübner, T. Staab, and R. Krause-Rehberg, Appl. Phys. A **61**, 203 (1995).

39 Y. Xin, E. M. James, I. Arslan, S. Sivananthan, N. D. Browning, S. J. Pennycook, F. Omnès, B. Beaumont, J.-P. Faurie, and P. Gibart, Appl. Phys. Lett. **76**, 466 (2000).

40 S. Pöykkö, M. J. Puska, and R. M. Nieminen, Phys. Rev. B **57**, 12174 (1998).

41 G. D. Watkins, Phys. Rev. Lett. **33**, 223 (1974).

42 K. Saarinen, T. Laine, K. Skog, J. Mäkinen, P. Hautojärvi, K. Rakennus, P. Uusimaa, A. Salokatve, and M. Pessa, Phys. Rev. Lett. **77**, 3407 (1996).

43 L. Liszkay, C. Corbel, and P. Hautojärvi, Appl. Phys. Lett. **70**, 2723 (1997).

44 T. Miyajima, H. Okuyama, K. Akimoto, and Y. Mori, Appl. Phys. Lett. **59**, 1482 (1991).

45 L. Wei, Y. K. Cho, C. Dosho, S. Tanigawa, T. Yodo, and K. Yamashita, Jpn. J. Appl. Phys. **30**, 2442 (1991).

46 F. Plazaola, A. P. Seitsonen, and M. J. Puska, J. Phys.: Condens. Matter **6**, 8809 (1994).

47 D. B. Laks, C. G. Van de Walle, G. F. Neumark, P. E. Blöchl, and S. T. Pantelides, Phys. Rev. B **45**, 10965 (1992).

48 M. J. Puska, C. Corbel, and R. M. Nieminen, Phys. Rev. B **41**, 9980 (1990).

49 J. Oila, K. Saarinen, T. Laine, P. Hautojärvi, P. Uusimaa, M. Pessa, and J. Likonen, Physica B **273-274**, 902 (1999).

50 H. Kobayashi, K. Kimura, F. Nishiyama, S. Miwa, and T. Yao, J. Cryst. Growth **184/185**, 475 (1998).

51 S. Kuisma, K. Saarinen, P. Hautojärvi, C. Corbel, and C. LeBerre, Phys. Rev. B **53**, 9814 (1996).